Check for updates

ChemistryEurope
Excellence in Chemistry Research Worldwide

Research Article
doi.org/10.1002/ceur.202500082

www.journal.chemistry-europe.org

Highly Shielded Peroxo-Cerium(IV)-Containing Polyoxometalate: Synthesis, Structure, and Oxidative Studies

Anusree Sundar, Danica Bajuk-Bogdanović, Gordana Ćirić-Marjanović, Talha Nisar, Veit Wagner, Arnulf Materny, Geoffrey B. Jameson, Bassem S. Bassil, and Ulrich Kortz*

The peroxo-bridged di-cerium(IV)-di-lithium-containing polyoxometalate $[(Ce^{IV}_2O_2)Li_2(P_2W_{16}O_{59})_2]^{16-}$ (**$Ce_2Li_2P_4W_{32}$**) is synthesized in a one-pot aqueous synthetic procedure and isolated as a hydrated mixed alkali salt, $K_{13.6}Na_{1.4}Li[(Ce^{IV}_2O_2)Li_2(P_2W_{16}O_{59})_2]\cdot 32H_2O$ (**KNaLi-$Ce_2Li_2P_4W_{32}$**). The novel polyanion **$Ce_2Li_2P_4W_{32}$** comprises a side-on peroxo-group bridging two cerium(IV) and two lithium ions, which are encapsulated between two dilacunary, face-on $\{P_2W_{16}\}$ Wells–Dawson units, with a vacant site in each of the two belts. The polyanion **$Ce_2Li_2P_4W_{32}$** is characterized in the solid state by single-crystal X-ray diffraction, Fourier transform infrared spectroscopy, thermogravimetric analysis, X-ray photoelectron spectroscopy, and Raman spectroscopy and in solution by ^{31}P NMR and Raman spectroscopy, respectively. **$Ce_2Li_2P_4W_{32}$** and the peroxo-group are shown to be highly stable in a large pH range and up to almost boiling temperatures, but at the same time the polyanion is reactive toward oxidation of triphenylphosphine, involving the peroxo group and the cerium(IV) centers.

1. Introduction

Polyoxometalates (POMs) are polynuclear, anionic metal-oxo complexes, which can often be formed from simple inorganic oxoanions by condensation reactions in aqueous, acidic media. Transition metals of groups 5 and 6 in high oxidation states can form POMs with main structural building blocks being the MO_6 octahedra, which are mostly corner or edge shared.[1] Peroxo-derivatives of POMs have been known since 1985, when Venturello and co-workers reported the peroxo-tungstophosphate $[PO_4\{WO(O_2)_2\}_4]^{3-}$, comprising a central phosphate ion surrounded by four oxo-di-peroxo-tungsten(VI) units.[2] This was followed by the synthesis of several peroxo-POMs, where the peroxo groups are bound to addenda atoms of the POM skeleton such as (the isopolyniobate $[H_3Nb_6O_{13}(O_2)_6]^{5-}$,[3] and the heteropolytungstates $[AsO_4\{W_2O_2(\mu\text{-}O_2)_2(O_2)_2\}_2]^{3-}$ and β_3-$[(Co^{II}O_4)W_{11}O_{31}(O_2)_4]^{10-}$.[4] This area further developed when peroxo-containing heteropolyanions were reported with the peroxo-groups being bound to the incorporated transition metal ions such as Nb^V, Zr^{IV}, and Hf^{IV}.[5]

The class of lanthanide-containing POMs was developed systematically by Pope[6] and later also Francesconi,[7] whereas Burns[8] succeeded in the preparation of peroxo-uranyl-based polyanions. More recently, the first example of a peroxo-Ce-containing POM was reported by Kortz, with a nona-peroxo-hexa-cerium(IV)-containing cyclic core coordinated by three $[GeW_{10}O_{37}]^{10-}$ fragments, leading to $[Ce_6(O_2)_9(GeW_{10}O_{37})_3]^{24-}$, which was active in selective thioether oxidation.[9]

POMs in general, and in particular peroxo-derivatives, are highly attractive in oxidation catalysis, such as for selective alkene epoxidation, alcohol oxidation, or for sulfoxidation with H_2O_2.[5,9,10] Peroxo-groups attached to transition metal centers can often serve as robust precursors for highly reactive intermediates, such as hydroperoxo species of the type POM-MOOH, hence becoming an active site for H_2O_2 activation which is then utilized for various H_2O_2-based oxidation catalysis. Lacunary POMs hosting the guest metal-peroxo unit are believed to stabilize such entity toward unwanted decomposition. However, there are no systematic studies addressing the extent to which POM encapsulation can enhance the stability of peroxo groups, nor how this may affect their thermal stability, solution stability, or reactivity when a redox-active metal-peroxo group is incorporated in a POM structure, with the redox-active metal site actively taking part in oxidations by accepting electrons.[11]

A. Sundar, T. Nisar, V. Wagner, A. Materny, B. S. Bassil, U. Kortz
School of Science
Constructor University
Campus Ring 1, 28759 Bremen, Germany
E-mail: ukortz@constructor.university

D. Bajuk-Bogdanović, G. Ćirić-Marjanović
Faculty of Physical Chemistry
University of Belgrade
Studentski trg 12-16, 11158 Belgrade, Serbia

T. Nisar
Institute of Advanced Ceramics
Integrated Materials Systems Group
Hamburg University of Technology
21073 Hamburg, Germany

G. B. Jameson
School of Food Technology and Natural Sciences
Massey University
Private Bag 11 222, Palmerston North 4442, New Zealand

Supporting information for this article is available on the WWW under https://doi.org/10.1002/ceur.202500082

© 2025 The Author(s). ChemistryEurope published by Chemistry Europe and Wiley-VCH GmbH. This is an open access article under the terms of the Creative Commons Attribution License, which permits use, distribution and reproduction in any medium, provided the original work is properly cited.

© 2025 The Author(s). ChemistryEurope published by Chemistry Europe and Wiley-VCH GmbH

Research Article
doi.org/10.1002/ceur.202500082

27514765, 2025, 4, Downloaded from https://chemistry-europe.onlinelibrary.wiley.com/doi/10.1002/ceur.202500082 by Technische Universität Hamburg Universitätsbibliothek, Wiley Online Library on [07/11/2025]. See the Terms and Conditions (https://onlinelibrary.wiley.com/terms-and-conditions) on Wiley Online Library for rules of use; OA articles are governed by the applicable Creative Commons License

In this work, we synthesized and investigated a peroxo-cerium(IV)-containing 32-tungsto-4-phosphate sandwich structure of the Wells–Dawson type, including structure and reactivity.

2. Results and Discussion

2.1. Synthesis and Structure

We have synthesized and structurally characterized the novel peroxo-cerium(IV) polyanion $[(Ce^{IV}_2O_2)Li_2(P_2W_{16}O_{59})_2]^{16-}$ (**$Ce_2Li_2P_4W_{32}$**) in aqueous medium starting with a Ce^{III} salt and constructing a $\{P_2W_{16}O_{59}\}$ unit in situ from $[H_2P_2W_{12}O_{48}]^{12-}$ and Na_2WO_4 at pH 7.5. The title polyanion **$Ce_2Li_2P_4W_{32}$** comprises a central peroxo-di-cerium(IV)-di-lithium group, which is encapsulated by two dilacunary $\{P_2W_{16}\}$ units, see **Figure 1**. The latter can be visualized as being formed from the parent $\{P_2W_{18}\}$ unit by removal of a WO_6 octahedron from each of the two belts. Such $\{P_2W_{16}\}$ fragment is very rarely observed, one example being a dimeric non-peroxo polyanion with four central Ce^{3+} ions reported by Pope's group.[6] The $\{P_2W_{16}\}$ unit with C_s symmetry has not been observed yet as an independent ion, despite not violating the Lipscomb rule.[12] As reported in the original investigation on lacunary derivatives of the Wells–Dawson ion by Massart and coworkers, the metastable, monolacunary belt-deficient α_1-isomer of $[P_2W_{17}O_{61}]^{10-}$ could be prepared only from the hexavacant $[H_2P_2W_{12}O_{48}]^{12-}$ ion.[13] In fact, **$Ce_2Li_2P_4W_{32}$** which comprises two Wells-Dawson fragments with such two belt vacancies was prepared analogously, but at a higher pH (7.5 vs. 4–5 for $\{\alpha_1$-$P_2W_{17}\}$), making use of the gradual reaction and incorporation of tungsten from Na_2WO_4 into the hexavacant $\{H_2P_2W_{12}\}$. The addition of Ce^{III} as well as H_2O_2 following the in situ formation of $\{\alpha_1$-$P_2W_{16}\}$ resulted in the oxidation of Ce^{III} to Ce^{IV} by H_2O_2. The +4-oxidation state of Ce was confirmed by bond valence sum calculations[14] and XPS (see Table S1 and Figure S1, Supporting Information). The resultant **$Ce_2Li_2P_4W_{32}$** was crystallized and then recrystallized for further purification to obtain a mixed K^+, Li^+, and Na^+ salt, which was confirmed by elemental analysis, resulting in the formula unit $K_{13.6}Na_{1.4}Li[(Ce^{IV}_2O_2)Li_2(P_2W_{16}O_{59})_2]\cdot 32H_2O$ (**KNaLi-$Ce_2Li_2P_4W_{32}$**). The crystal water content was determined by TGA (Figure S2, Supporting Information) and elemental analysis. Single-crystal XRD (see crystallographic data in **Table 1**) revealed that the two $\{P_2W_{16}\}$ units are connected via two 8-coordinated Ce^{IV} ions and two square-pyramidally coordinated lithium ions, which are bridged via a side-on peroxo group. This is a rare case where lithium ions could be located by XRD (see Figure 1, right).[15] The Li ions are linked to the Ce-coordinated peroxo moiety and by oxo-bridges to P and W centers. This core resembles the coordination in Pope's cerium(III)-containing $[Ce^{III}_4(OH)_2(H_2O)_9(P_2W_{16}O_{59})_2]^{14-}$ where two additional cerium ions occupy the positions of the two Li^+ ions in **$Ce_2Li_2P_4W_{32}$**.[6] The peroxo group in **$Ce_2Li_2P_4W_{32}$** is encapsulated by two bulky $\{P_2W_{16}\}$ units and hence very well protected from the environment. The O—O bond length in the peroxo group is 1.50 Å and the distance between the two Ce^{IV} ions is 4.40 Å.

The FTIR spectrum of **KNaLi–$Ce_2Li_2P_4W_{32}$** shows bands which correspond to the vibrations ν_{as}[P—O_a] (1117, 1077 and 1022 cm^{-1}), ν_{as}[W═O_d] (943 and 922 cm^{-1}), and ν_{as}[W—O_b—W] (793 and 737 cm^{-1}) (Figure S3, Supporting Information).[16] As the POM unit $\{P_2W_{16}\}$ seen in **KNaLi-$Ce_2Li_2P_4W_{32}$** has so far not been isolated as a free ion, we do not have an IR spectrum of it for comparison. However, the spectrum resembles the monolacunary P_2W_{17} (Figure S3, Supporting Information black), especially in the P—O_a and ν_{as}[W═O_d] region. The intensity of the band at 1117 cm^{-1} of the phosphate hetero group is strong for **KNaLi-$Ce_2Li_2P_4W_{32}$** and consistent with the presence of two α_1-type lacunary sites. For comparison, the corresponding phosphate band of P_2W_{12} appears at 1130 cm^{-1}.[14] The weak bands seen at 843 and 633 cm^{-1} in the spectrum of **KNaLi-$Ce_2Li_2P_4W_{32}$** can be ascribed to the stretching vibration of the O—O and Ce—O_{peroxo} groups respectively.[17] There could be a possible influence of the adjacent Li—O bond to the ν(O—O) band. It can be speculated that a slight asymmetry (the lack of rigorous symmetry) in **KNaLi-$Ce_2Li_2P_4W_{32}$**, possibly due to the existence of different conformation, could result in changes in geometry and electronic structure. This asymmetry might result from interactions between the POM and the three different counter cations (K^+, Li^+, and Na^+), and/or from hydrogen bonding with H_2O, thus resulting in the appearance of a weak O—O stretching band in the

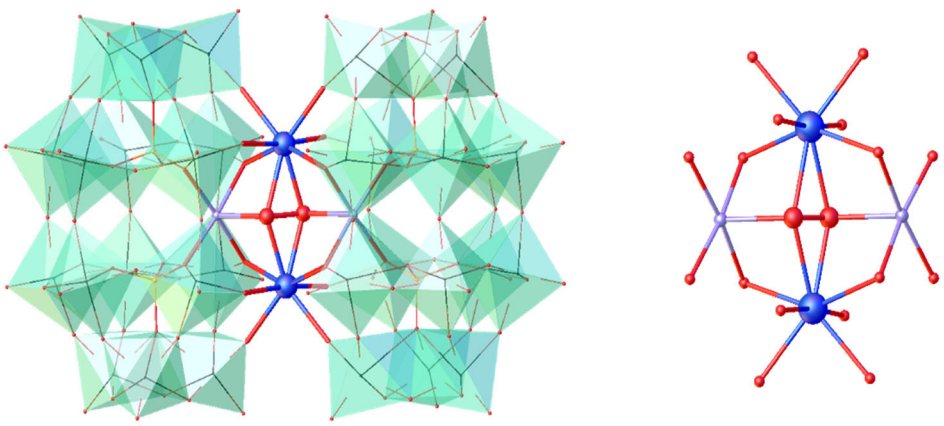

Figure 1. (Left) Combined polyhedral/ball-and-stick representation of **$Ce_2Li_2P_4W_{32}$** (right). View of the coordination environment of the two lithium ions in the central **$Ce_2Li_2P_4W_{32}$** core. Color code: WO_6 octahedra (turquoise), P (orange), Ce^{IV} (blue), Li (lilac), and O (red).

© 2025 The Author(s). ChemistryEurope published by Chemistry Europe and Wiley-VCH GmbH

Research Article
doi.org/10.1002/ceur.202500082

27514765, 2025, 4, Downloaded from https://chemistry-europe.onlinelibrary.wiley.com/doi/10.1002/ceur.202500082 by Technische Universität Hamburg Universitätsbibliothek, Wiley Online Library on [07/11/2025]. See the Terms and Conditions (https://onlinelibrary.wiley.com/terms-and-conditions) on Wiley Online Library for rules of use; OA articles are governed by the applicable Creative Commons License

Table 1. Crystallographic data for $K_{13.6}Na_{1.4}Li[Ce^{IV}_2O_2)Li_2(P_2W_{16}O_{59})_2]\cdot 32H_2O$ (**KNaLi–$Ce_2Li_2P_4W_{32}$**).

Chemical formula	$Ce_2KLi_2NaO_{122}P_4W_{32}$
Formula weight	8291.97
Temperature/K	173.15
Crystal system	Triclinic
Space group	P-1 ($Z = 1$)
a/Å	12.79790(10)
b/Å	15.31760(10)
c/Å	20.4259(2)
α/°	75.6010(10)
β/°	73.5910(10)
γ/°	77.9060(10)
Volume/Å^3	3678.37(6)
Z	1
ρ_{calc}g/cm^3	3.7431
μ/mm^{-1}	25.664
F(000)	3530.9
Crystal size/mm^3	0.13 × 0.10 × 0.07
Radiation/ Å	Mo Kα ($\lambda = 0.71073$)
2Θ range for data collection/°	6.82 to 63.02
Completeness	99.8%
Reflections collected	242 169
Independent reflections	24 448 [$R_{int} = 0.0605$, $R_{sigma} = 0.0309$, $R_{sigma} = 0.0309$]
Data/restraints/ parameters	24 448/366/726
Goodness-of-fit on F^2	0.959
Final R indexes [I>=2σ (I)][a]	$R_1 = 0.0273$, w$R_2 = 0.0719$
Final R indexes [all data][b]	$R_1 = 0.0334$, w$R_2 = 0.0753$

[a]$R = \Sigma||F_o| - |F_c||/\Sigma|F_o|$. [b]$R_w = [\Sigma w(F_o^2 - F_c^2)^2/\Sigma w(F_o^2)^2]^{1/2}$. The structure (see chemical formula, which included a single well-defined K^+ and two attached water molecules), was "SQUEEZEd" using the protocol in OLEX2, yielding a single-void volume of 1569 Å^3 containing 769 e$^-$. With respect to the formula deduced from microanalytical data, given in the Table, there are 543 e$^-$ not included in the chemical formula. The difference of 226 e$^-$ is attributed to ≈22 labile water molecules that are lost prior to TGA and microanalysis, but not from the freshly harvested sample for X-ray data collection.

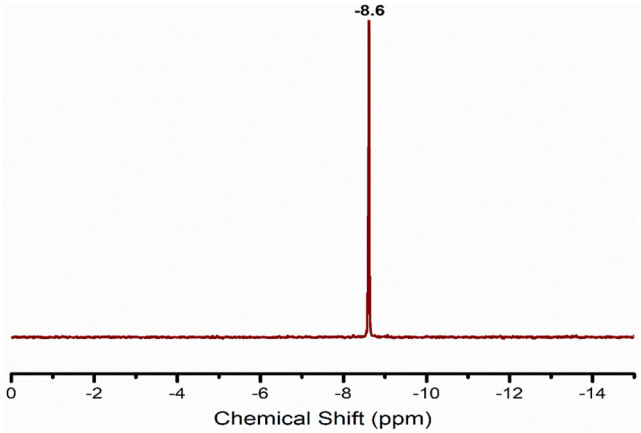

Figure 2. Room-temperature ^{31}P NMR spectrum of **KNaLi–$Ce_2Li_2P_4W_{32}$** dissolved in H_2O.

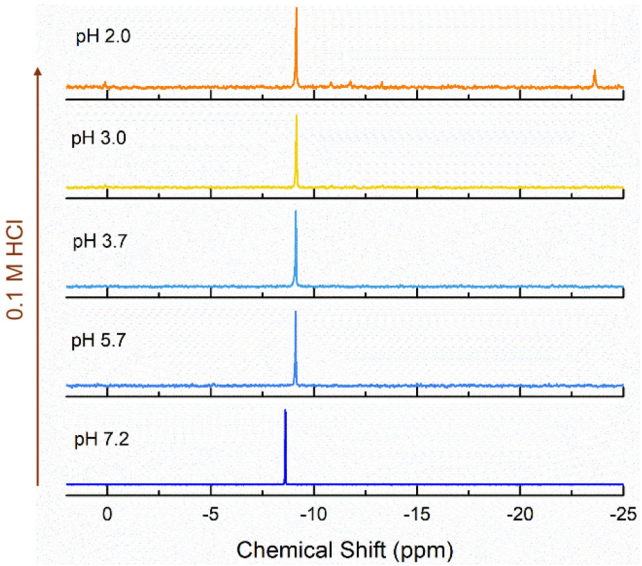

Figure 3. ^{31}P NMR spectra of **$Ce_2Li_2P_4W_{32}$** dissolved in water with pH adjustment from 7.2 until 2.0 with 0.1 M HCl_{aq}.

FTIR spectrum, despite the crystallographic centre of symmetry in the crystal structure, which reports only the average conformation and composition. In addition, as discussed below, this band may arise from a combination with the allowed Li-O(peroxo) band.[17] The solid-state and solution Raman spectra for this sample were also measured and their close similarity confirms that the title polyanion $[(Ce^{IV}_2O_2)Li_2(P_2W_{16}O_{59})_2]^{16-}$ (**$Ce_2Li_2P_4W_{32}$**) characterized structurally in the solid state pertains also to the solution state. Detailed spectra are provided in the Supporting Information Figures S5 and S6, Supporting Information). The ^{31}P NMR spectrum of **KNaLi–$Ce_2Li_2P_4W_{32}$** dissolved in water resulted in a clean singlet at −8.6 ppm (see **Figure 2**). This is in accordance with the four structurally and magnetically equivalent P atoms in the structure. The spectrum remained unchanged for several weeks, indicating a very high stability of **$Ce_2Li_2P_4W_{32}$** in solution.

2.2. pH Stability

The pH stability window of **$Ce_2Li_2P_4W_{32}$** in water was monitored using ^{31}P NMR, starting from a pH of 7.2, which corresponds to the pH of a solution prepared by dissolving 50 mg of **KNaLi–$Ce_2Li_2P_4W_{32}$** in 1 mL of water. This solution was gradually acidified with 0.1 M HCl to lower the pH to the target value. The NMR spectrum (**Figure 3**) indicates that **$Ce_2Li_2P_4W_{32}$** remains stable within a pH range of 7.2–2.0, with only slight decomposition observed at pH 2. The slight upfield shift of the signal is due to the pH change. Details of the pH changes upon HCl addition, H^+ consumption, and monitoring of POM decomposition at pH 2 and below are given in detail in SI, Section 5.

© 2025 The Author(s). ChemistryEurope published by Chemistry Europe and Wiley-VCH GmbH

Research Article
doi.org/10.1002/ceur.202500082

27514765, 2025, 4, Downloaded from https://chemistry-europe.onlinelibrary.wiley.com/doi/10.1002/ceur.202500082 by Technische Universität Hamburg Universitätsbibliothek, Wiley Online Library on [07/11/2025]. See the Terms and Conditions (https://onlinelibrary.wiley.com/terms-and-conditions) on Wiley Online Library for rules of use; OA articles are governed by the applicable Creative Commons License

3. Thermal Stability Studies in Solid and Solution States

3.1. ^{31}P NMR Spectroscopy

In order to investigate the thermal stability of **$Ce_2Li_2P_4W_{32}$** as well as the stability of the peroxo group inside the structure, we monitored the ^{31}P NMR spectrum of the polyanion in water from room temperature up to 90 °C. A singlet was observed throughout, indicating a high stability of the polyanion in water even at high temperature (see **Figure 4**, left). We observed a gradual downfield shift of the singlet in ^{31}P NMR spectra with increasing temperature, as seen in Figure 4. To examine whether this shift is due to any structural change or peroxo decomposition, we measured the ^{31}P NMR spectra of the same solution after repeated heating and cooling. As shown in Figure 4, right, the chemical shift of the peak returns to its original position after the solution is cooled down to room temperature. The same peak shift was observed after heating and consecutively cooling the solution multiple times. This clearly demonstrates that the title polyanion **$Ce_2Li_2P_4W_{32}$** remains intact throughout.

3.2. Raman Spectroscopy

Solid-state and solution Raman studies were conducted to further validate the thermal stability of **$Ce_2Li_2P_4W_{32}$**, with a particular focus on assessing the thermal stability of the central peroxo group, which cannot be monitored via NMR spectroscopy. Heating a solid sample of **KNaLi–$Ce_2Li_2P_4W_{32}$** was done using two methods: 1) conventional heating of the sample and 2) varying the laser power (Section 6.1 in SI).

The Raman spectrum of **KNaLi-$Ce_2Li_2P_4W_{32}$** in the solid state at room temperature shows two strong bands at 982 cm^{-1} and 962 cm^{-1} which are assigned to the symmetric and asymmetric W═O_d stretching vibrations, ν_{sym}(W═O_d) and ν_{asym}(W═O_d), respectively, and two weaker bands at 837 cm^{-1} and 647 cm^{-1}, indicative of the cerium-peroxo group and attributable to O—O stretching in the Ce-peroxo Ce(O_2) group, ν(O—O), and symmetric Ce—O stretching, ν_{sym}(Ce—O), respectively (Figure S5, Supporting Information).[18] The origin of the band at 878 cm^{-1} is under consideration. It is at a position of the O—O stretching band in free H_2O_2 which appears at 875 cm^{-1}.[19] Therefore, this band could be an indication of the formation of an H_2O_2 adduct with the POM.[20]

A comparison of the Raman spectra of **KNaLi-$Ce_2Li_2P_4W_{32}$** recorded at two different locations on the solid sample after thermal treatment at 50 °C (see **Figure 5**, left) and at 90 °C (see Figure 5, right) showed that the same bands (and at almost the same positions) are present in the spectra for both temperatures, indicating good thermal stability of the compound. It is an important observation that the bands assigned to the Ce(O_2) group at 837 and 647 cm^{-1} remained unchanged upon heating at 50 and 90 °C, indicating good thermal stability of the cerium-peroxo group inside **$Ce_2Li_2P_4W_{32}$**. There is no indication of any decomposition of the polyanion to other species.

Raman spectra of aqueous solutions of **$Ce_2Li_2P_4W_{32}$** at two different concentrations at (1) room temperature and 2) after thermal treatment up to 50 °C and 90 °C are shown in **Figure 6**. For both concentrations the spectra at all studied temperatures are almost identical regarding the positions and relative intensities of the bands, indicating excellent thermal stability of **$Ce_2Li_2P_4W_{32}$** in the solution state, confirming our ^{31}P NMR results (*vide supra*). As in the case of the solid state, the bands assigned to the Ce(O_2) group at 837 and 641 cm^{-1} remained unchanged upon heating the solutions to 50 and 90 °C, respectively, indicating excellent thermal stability of the cerium-peroxo group inside the **$Ce_2Li_2P_4W_{32}$** structure in the solution state. There is no indication of any decomposition of **$Ce_2Li_2P_4W_{32}$** under the conditions studied.

Also, the Raman spectra for solutions of **$Ce_2Li_2P_4W_{32}$** contained the characteristic bands at the same or very similar positions (977, 967, 837, and 641 cm^{-1}, see Figure 6) to those seen in the solid state (982, 969, 837, and 647 cm^{-1}, Figure S5, Supporting

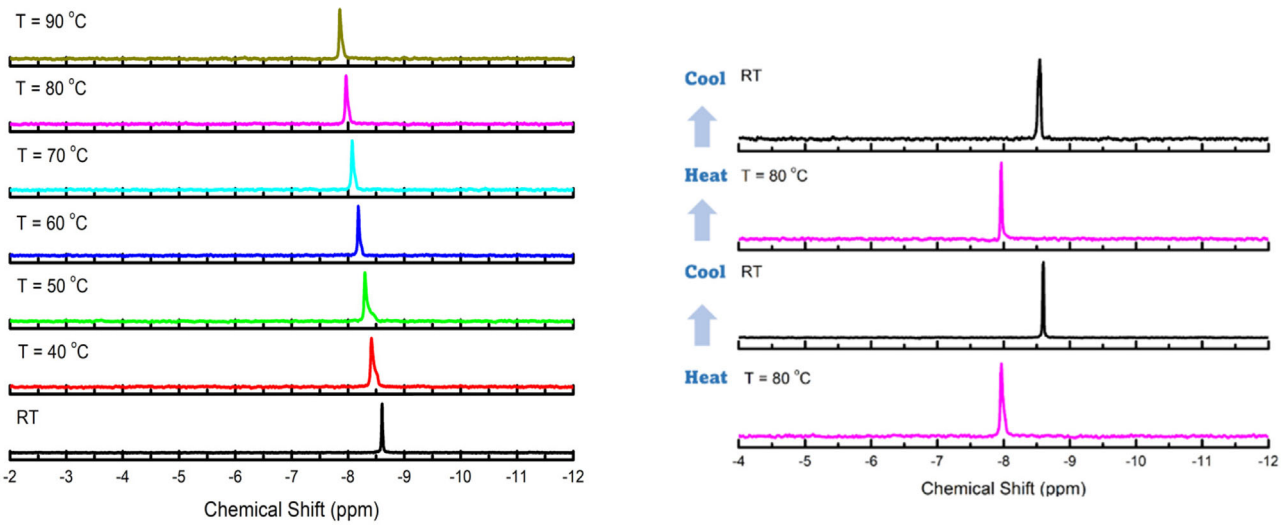

Figure 4. (Left) Temperature-dependent ^{31}P NMR spectra of **$Ce_2Li_2P_4W_{32}$** in H_2O/D_2O; (right) ^{31}P NMR spectra of **$Ce_2Li_2P_4W_{32}$** in H_2O/D_2O after heating and cooling cycles (RT = room temperature), indicating complete reversibility of the chemical shift changes.

© 2025 The Author(s). ChemistryEurope published by Chemistry Europe and Wiley-VCH GmbH

Research Article
doi.org/10.1002/ceur.202500082

27514765, 2025, 4, Downloaded from https://chemistry-europe.onlinelibrary.wiley.com/doi/10.1002/ceur.202500082 by Technische Universitat Hamburg Universitatsbibliothek, Wiley Online Library on [07/11/2025]. See the Terms and Conditions (https://onlinelibrary.wiley.com/terms-and-conditions) on Wiley Online Library for rules of use; OA articles are governed by the applicable Creative Commons License

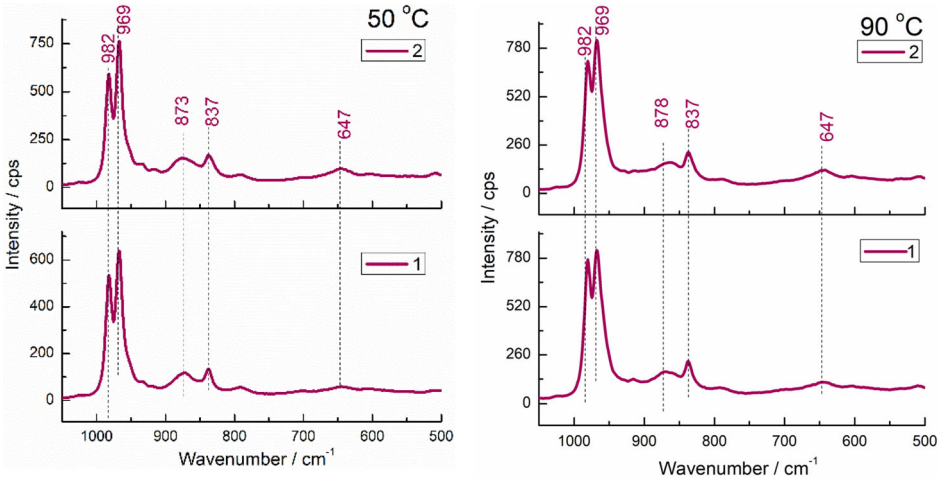

Figure 5. Raman spectra of **KLiNa–$Ce_2Li_2P_4W_{32}$** in the solid state after thermal treatment at 50 °C (left) and 90 °C (right), recorded at two different locations (1, and 2) on the sample (laser power 1 mW).

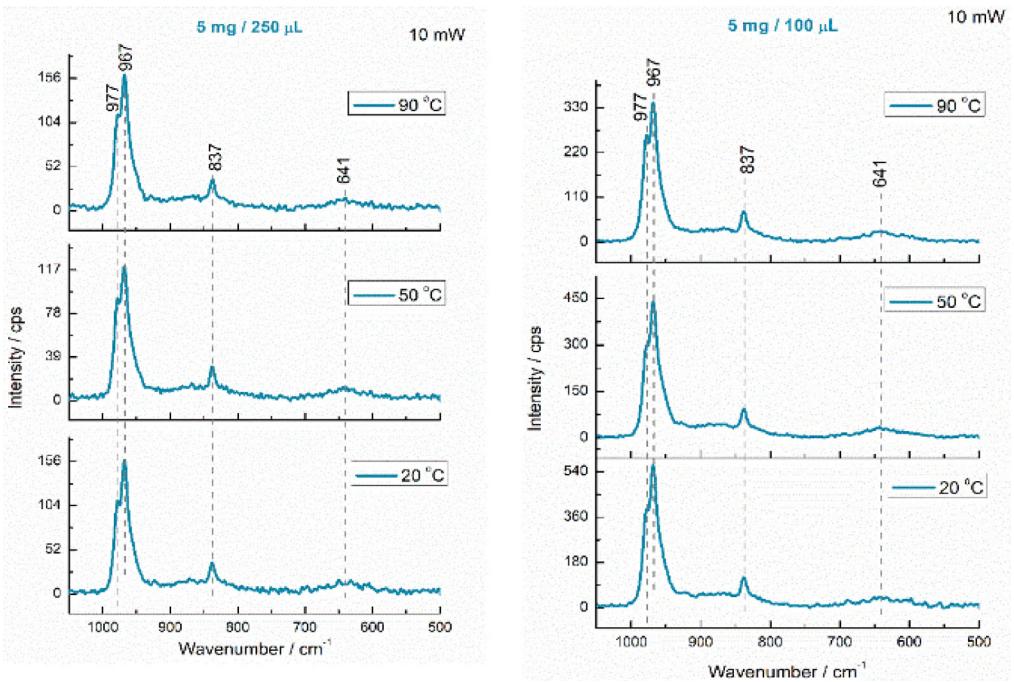

Figure 6. Raman spectra of aqueous solutions of **$Ce_2Li_2P_4W_{32}$** at two different concentrations (5 mg 100 µL and 5 mg 250 µL) at room temperature (bottom) and after thermal treatment up to 50 °C (middle) and 90 °C (top), recorded with a laser power of 10 mW.

Information), indicating a high stability of the title polyanion, independent of its physical state.

The absence of changes in the relative intensity of the two ν(W═O) bands (982 and 969 cm^{-1}) with an increase of the solution temperature (Figure 6) supports our previous assumptions about the origin of these changes when the Raman spectrum was recorded for the sample in the solid state (loss of solvent and/or hydration water).

Furthermore, we were able to successfully recrystallize **KNaLi-$Ce_2Li_2P_4W_{32}$** from an aqueous solution after heating to boiling, with the polyanion and the peroxo group fully intact. This provides further support for our assertion regarding compound stability.

4. Chemical Reactivity of Peroxo Group

As discussed so far, the polyanion **KNaLi-$Ce_2Li_2P_4W_{32}$** contains a highly thermally stable peroxo group, effectively shielded by two bulky $[P_2W_{16}O_{59}]^{12-}$ units. This raises the question of whether the peroxo groups are accessible to substrates for oxidation or reactive enough to oxidize challenging substrates. To explore its suitability for catalytic applications, we evaluated the reactivity of the peroxo group in **$Ce_2Li_2P_4W_{32}$** using triphenylphosphine (PPh_3), a well-known peroxo-quenching agent. The study was performed by dissolving 2 equiv. PPh_3 in toluene and phase transferring 1 equiv. **$Ce_2Li_2P_4W_{32}$** into toluene from water using Aliquat336 (see

© 2025 The Author(s). ChemistryEurope published by Chemistry Europe and Wiley-VCH GmbH

Research Article
doi.org/10.1002/ceur.202500082

27514765, 2025, 4, Downloaded from https://chemistry-europe.onlinelibrary.wiley.com/doi/10.1002/ceur.202500082 by Technische Universität Hamburg Universitätsbibliothek, Wiley Online Library on [07/11/2025]. See the Terms and Conditions (https://onlinelibrary.wiley.com/terms-and-conditions) on Wiley Online Library for rules of use; OA articles are governed by the applicable Creative Commons License

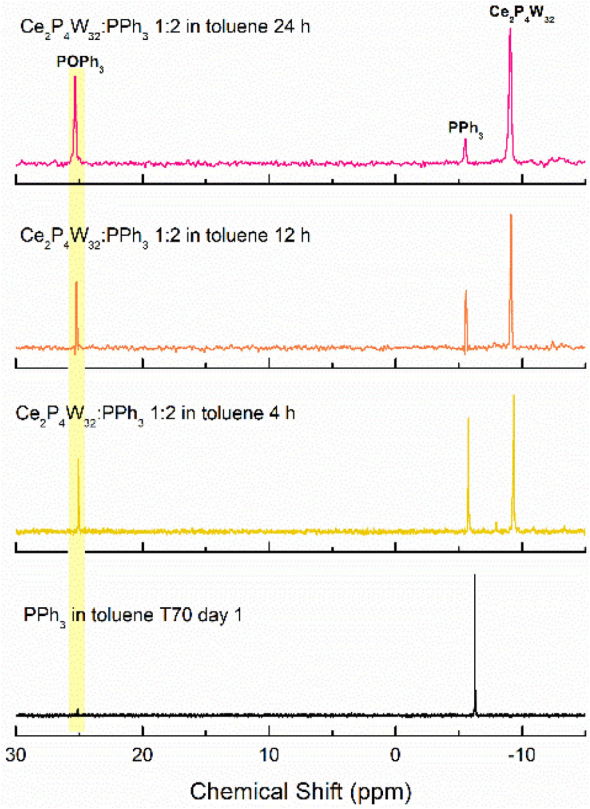

Figure 7. From bottom to top: ^{31}P NMR of PPh_3 in toluene after 1 day; $\mathbf{Ce_2Li_2P_4W_{32}}$ and PPh_3 in toluene after 4 h; after 12 h; and 24 h of mixing. All solutions maintained at 70 °C in a closed system.

details in the Experimental Section). The reaction was monitored over several days using ^{31}P NMR spectroscopy. Although the reaction proceeded slowly and the rate of the reaction was temperature dependent (Figure S10, Supporting Information), which can be an indication of the peroxo-POM being a weak electrophile, the formation of $POPh_3$ ($\delta = 25.4$ ppm) was observed (**Figure 7**). When the system was stirred vigorously at 70 °C for 4 h, we observed 40% oxidation of PPh_3 to $POPh_3$ (calculated by integration of ^{31}P NMR signals) and by 24 h it reached 77% (1.6 equiv.), as determined by peak integration (integrated spectra shown in Figures S11 and S12, Supporting Information respectively). The observation that a higher equivalence of PPh_3 is oxidized from $+3$ to $+5$, exceeding the expected 1 equivalent for a single peroxo group capable of accepting an additional 2 electrons, is *a priori* unexpected. This can only be rationalized if both Ce^{IV} centers in the polyanion participate in the redox reaction by accepting an additional 2 electrons (being reduced from Ce^{IV} to Ce^{III}). Hence, we propose that the peroxo group and the two Ce^{IV} ions in $\mathbf{Ce_2Li_2P_4W_{32}}$ actively participate in the oxidation of PPh_3 to $POPh_3$. The oxidation state of cerium after reaction of $\mathbf{Ce_2Li_2P_4W_{32}}$ with PPh_3 was identified by XPS (**Figure 8**). A *3d* doublet peak was observed, resulting from the spin-orbit split core level with *j* quantum numbers of 3/2 and 5/2. An additional peak, at a binding energy of 916.7 eV (highlighted in yellow), which typically arises from hybridization of the *4f* state with the *2p* orbital of the ligand in Ce^{IV} (see Figure S1, Supporting Information), is absent here.

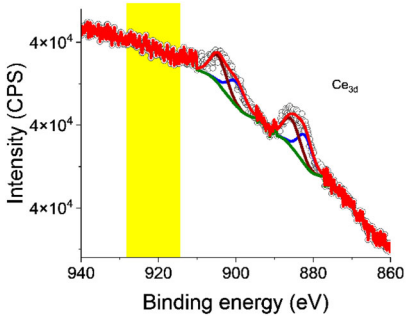

Figure 8. Photoelectron spectra and fits for Ce $3d_{5/2}$ and $3d_{3/2}$ multiplets of $\mathbf{Ce_2Li_2P_4W_{32}}$ after reaction with PPh_3.

This absence indicates that cerium has been reduced to Ce^{III} after reaction with PPh_3, confirming our hypothesis. The absence of Ce^{IV} in the XPS spectra, despite only 1.6 equivalents of PPh_3 being oxidized (rather than 2 equivalents), is attributed to the time delay between the NMR and XPS measurements. By the time XPS was measured all the PPh_3 was oxidized to $POPh_3$, as confirmed by the ^{31}P NMR spectrum of the sample taken after the XPS measurement and dissolved in toluene (Figure S13, Supporting Information).

Another noteworthy observation is the rate of PPh_3 oxidation, which is higher during the initial phase of the reaction (≈50% oxidation) before slowing down. This behavior suggests that the initial rapid oxidation may be driven by facile peroxo quenching, followed by a slower oxidation process likely associated with the reduction of cerium.

We propose the following reactions.

$$[(Ce^{IV}{}_2O_2)Li_2(P_2W_{16}O_{59})_2]^{16-} + PPh_3 + H_2O \rightarrow [(Ce^{IV}{}_2(OH)_2)Li_2(P_2W_{16}O_{59})_2]^{16-} + POPh_3 \quad (1)$$

($2e^-$ *reduction of the peroxo group*)

$$[(Ce^{IV}{}_2(OH)_2)Li_2(P_2W_{16}O_{59})_2]^{16-} + PPh_3 + H_2O \rightarrow [H_x(Ce^{III}{}_2(OH)_2)Li_2(P_2W_{16}O_{59})_2]^{(18-x)-} + POPh_3 \quad (2)$$

($2e^-$ *reduction of the 2* Ce^{IV} *centers*)

In the above reactions we assume that the O atoms originate from water molecules in toluene, which was exposed to a lot of water in the beginning of the reaction, when $\mathbf{Ce_2Li_2P_4W_{32}}$ was transferred from the aqueous to the organic phase.

Unfortunately, we were not successful in isolating and crystallizing the peroxo-depleted and reduced form of $\mathbf{Ce_2Li_2P_4W_{32}}$, and hence we cannot confirm with absolute confidence the above proposed formula of the peroxo-depleted polyanion. We also observed that attempting to regenerate the peroxo-POM by adding an excess of 30% H_2O_2 leads to the decomposition of $\mathbf{Ce_2Li_2P_4W_{32}}$. This decomposition is attributed to the acidification of the solution caused by H_2O_2, which lowers the pH beyond the stability range of the polyanion.

A control reaction with PPh_3 in toluene that was exposed to water maintained at 70 °C, in the absence of $\mathbf{Ce_2Li_2P_4W_{32}}$, showed negligible air oxidation of PPh_3 over the same time period (bottom spectrum, Figure 7). This confirms that the observed formation of $POPh_3$ arises from reaction with the title polyanion.

© 2025 The Author(s). ChemistryEurope published by Chemistry Europe and Wiley-VCH GmbH

Research Article
doi.org/10.1002/ceur.202500082

27514765, 2025, 4, Downloaded from https://chemistry-europe.onlinelibrary.wiley.com/doi/10.1002/ceur.202500082 by Technische Universität Hamburg Universitätsbibliothek, Wiley Online Library on [07/11/2025]. See the Terms and Conditions (https://onlinelibrary.wiley.com/terms-and-conditions) on Wiley Online Library for rules of use; OA articles are governed by the applicable Creative Commons License

Importantly, the peak at $\delta = -9.1$ ppm, assigned to **$Ce_2Li_2P_4W_{32}$**, shows a slight broadening after the peroxo-quenching reaction, but could not be resolved to two individual peaks. The peroxo-depleted **$Ce_2Li_2P_4W_{32}$** exhibited minimal changes in the chemical environment of the phosphate moieties within the POM, as evidenced by ^{31}P NMR. This is likely attributable to a long (five-bonds) distance between the phosphorus atoms and the peroxo group within the structure. This also indicates that the peroxo depletion does not compromise the structural integrity of the POM. Thus, the peroxo-depleted **$Ce_2Li_2P_4W_{32}$** is structurally stable, but the subtle changes occurring during the depletion process are difficult to resolve by ^{31}P NMR spectroscopy alone.

Therefore, we decided to monitor the depletion of the peroxo-group in **$Ce_2Li_2P_4W_{32}$** while reacting with PPh_3 by Raman spectroscopy. Monitoring the reaction in a single-phase system via solution Raman spectroscopy was found to be challenging (see SI for Raman spectra on this reaction). The intense bands of toluene and PPh_3 mask the weaker O—O vibrations in the Raman spectra (Figure S14, Supporting Information). To address this, the setup was modified to a biphasic system with **$Ce_2Li_2P_4W_{32}$** in water and PPh_3 in toluene allowing for interaction between the two components via simple mixing of the immiscible phases. This modification significantly increased the reaction time, which is understandable, as the reaction occurs at the interface of the two phases rather than within a single homogeneous phase. The detailed experimental setup and the ^{31}P NMR monitoring of the biphasic setup are described in detail in the SI (section 7.2). The Raman spectrum of an air-dried drop from the aqueous phase containing **$Ce_2Li_2P_4W_{32}$** showed two bands at ≈840 and 640 cm^{-1} from the Ce-peroxo group and two characteristic very strong bands at ≈980 and 966 cm^{-1} due to the symmetric and asymmetric W═O_d stretching vibrations, respectively. A comparison of such solid-state Raman spectrum of the air-dried drop from the aqueous layer after 60 min versus 13 days showed a decrease in the relative intensity of the band at 836 cm^{-1} (ν(O—O) vibration of the $Ce_2(O_2)$ group after 13 days, which is an indication of the slow depletion of the peroxo-group in **$Ce_2Li_2P_4W_{32}$** (see **Figure 9**).

In order to shed more light on the reactivity of the peroxo group in **$Ce_2Li_2P_4W_{32}$**, we decided to perform a complementary investigation with FTIR spectroscopy in the solid state, which is a "bulk" analytical solid-state technique, by measuring FTIR spectra with time.

The FTIR spectra of solid **KNaLi-$Ce_2Li_2P_4W_{32}$** and the air-dried drop from the aqueous phase of the **$Ce_2Li_2P_4W_{32}$**-PPh_3 biphasic mixture recorded after $t = 12$ days are shown in **Figure 10**. The two spectra are very similar, implying the overall structural integrity of the polyanion, but the spectra also show some subtle differences. The main difference is the disappearance of the band at 841 cm^{-1}, assigned to the stretching vibration of the peroxo group (ν(O—O)) mixed with the ν(Li—O) stretching, in the spectrum of the air-dried drop from the aqueous phase of the **$Ce_2Li_2P_4W_{32}$**-PPh_3 biphasic mixture recorded after 12 days. This feature is a strong indication for the depletion of the peroxo-group in **$Ce_2Li_2P_4W_{32}$** after reaction with PPh_3 and is consistent with previous indications from solid-state Raman spectra via the band at 836 cm^{-1}. Another interesting feature is the modified relative intensity of the bands at 1076 and 1117 cm^{-1}, respectively, which correspond to the ν_{as}[P—O_a] vibrations. In the initial spectrum of **KNaLi-$Ce_2Li_2P_4W_{32}$** the band at 1117 cm^{-1} is stronger than that at 1076 cm^{-1}, whereas in the spectrum of the air-dried drop from the aqueous layer of the **$Ce_2Li_2P_4W_{32}$**-PPh_3 biphasic mixture the intensity ratio is reversed, and the band at 1076 cm^{-1} is stronger than that at 1117 cm^{-1}. This intensity change could be due to some subtle structural (re)organization of **$Ce_2Li_2P_4W_{32}$** upon depletion of the peroxo group by reaction with PPh_3. It is likely that the side-on bridging peroxo-group in **$Ce_2Li_2P_4W_{32}$** is replaced by two bridging hydroxo ligands, which will maintain the negative charge and lead to only minor structural changes in the core of the polyanion.

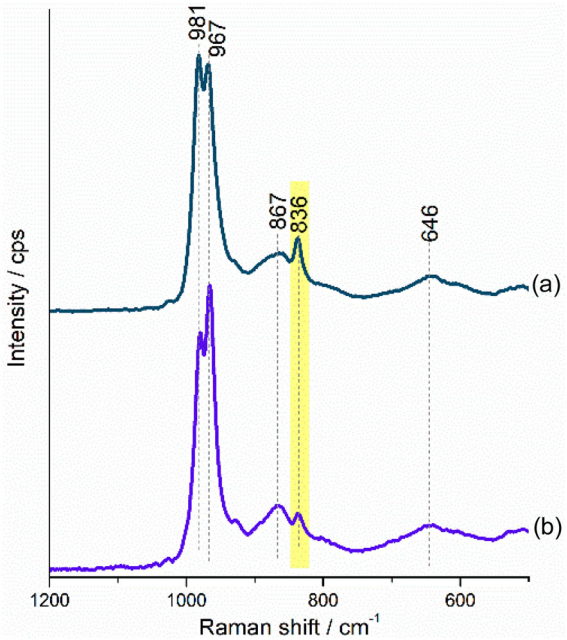

Figure 9. Solid-state Raman spectra of an air-dried drop from the aqueous phase of the biphasic **$Ce_2Li_2P_4W_{32}$**–PPh_3 system after a) 60 min and b) 13 days.

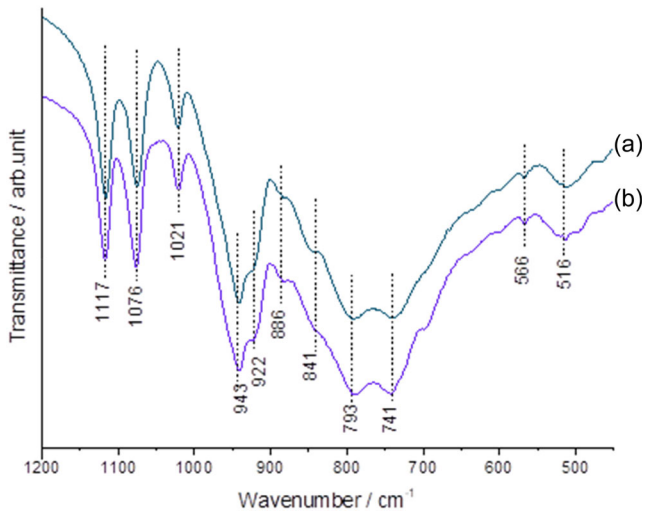

Figure 10. FTIR spectra of a) **KNaLi–$Ce_2Li_2P_4W_{32}$** in the solid state and b) an air-dried drop from the aqueous phase of the biphasic **$Ce_2Li_2P_4W_{32}$**–PPh_3 system recorded 12 days after mixing.

© 2025 The Author(s). ChemistryEurope published by Chemistry Europe and Wiley-VCH GmbH

Research Article
doi.org/10.1002/ceur.202500082

27514765, 2025, 4, Downloaded from https://chemistry-europe.onlinelibrary.wiley.com/doi/10.1002/ceur.202500082 by Technische Universität Hamburg Universitätsbibliothek, Wiley Online Library on [07/11/2025]. See the Terms and Conditions (https://onlinelibrary.wiley.com/terms-and-conditions) on Wiley Online Library for rules of use; OA articles are governed by the applicable Creative Commons License

This combined NMR and Raman/IR study demonstrates that the peroxo-group in **$Ce_2Li_2P_4W_{32}$** is still chemically active, in spite of being encapsulated by two large POM units, but at the same time the peroxo-group is strongly protected from thermal decomposition.

5. Conclusion

We have prepared the peroxo-cerium(IV)-containing 32-tungsto-4-phosphate $[(Ce^{IV}_2O_2)Li_2(P_2W_{16}O_{59})_2]^{16-}$ (**$Ce_2Li_2P_4W_{32}$**) comprising a side-on peroxo-group bridging two Ce^{IV} ions, encapsulated by two divacant $\{P_2W_{16}O_{59}\}$ Wells–Dawson groups with a vacancy in each of the two belts. The novel polyanion **$Ce_2Li_2P_4W_{32}$** and its central peroxo group demonstrate exceptional thermal and chemical stability in both the solid state and in solution, maintaining structural integrity across a broad pH range (7.0–2.0) and at temperatures approaching boiling, as confirmed by ^{31}P NMR and Raman spectroscopy. Despite being shielded by the bulky POM framework, the peroxo group in **$Ce_2Li_2P_4W_{32}$** remains chemically active, as evidenced by its reactivity with triphenylphosphine. The incorporation of Ce^{IV} as a redox-active metal in the peroxo-POM **$Ce_2Li_2P_4W_{32}$** further enhances the oxidative strength of the title polyanion beyond the activity of the peroxo group. These findings establish a strong foundation for further exploration of peroxo-polyoxometalates as robust and efficient peroxo-activation and oxidation sites, offering a stabilizing effect to peroxygens and broad potential for catalytic applications.

6. Experimental Section

Instrumentation

X-Ray Diffraction: Data were collected on a Rigaku XtaLAB Synergy, Dualflex, HyPix single-crystal diffractometer equipped with kappa geometry (graphite monochromator, $\lambda_{MoK\alpha} = 0.71073$ Å) using the CrysAlisPro software package.[21] An empirical absorption correction was applied using the ABSPACK program.[22] The structure was solved by direct methods, elaborated with the aid of successive difference Fourier maps and refined against all data using SHELXL-2014,[23] as embedded in OLEX2 version 1.5.[24] All refinements were conducted by full-matrix least squares against $|F|^2$ using all data. The heavy atoms were refined anisotropically, and Li and O atoms were refined anisotropically, but with sphericity restraints (ISOR 0.01 0.02 $O $Li). Three reflections at low resolution were omitted as they were partially occluded by the beam stop ($|F_{obs}| \ll |F_{calc}|$). The structure (see chemical formula in Table 1 ($Ce_2KLi_2NaO_{122}P_4W_{32}$), which included a single well-defined K^+ and two attached water molecules) was "SQUEEZEd" using the protocol in OLEX2, yielding a single-void volume of 1569 Å^3 containing 769 e$^-$. With respect to the formula deduced from microanalytical data, given in the heading, there were 543 e$^-$ not included in the chemical formula. The difference of 226 e$^-$ was attributed to ≈22 labile water molecules that were lost prior to TGA and microanalysis, but not from the freshly harvested crystals for X-ray data collection. Refinements were based upon the formula deduced from difference Fourier electron density maps ($K_{12}Na[Li_2Ce_2(O_2)P_4W_{32}O_{118}]25H_2O$) and resulted in $R1 = 0.0343$ and $wR2 = 0.0977$ for data with $I > 2\sigma(I)$ and to $R1 = 0.0434$ and $wR2 = 0.997$ for all data, being plagued by disordered cations and solvate structure. The images of the crystal structure were generated by Olex2, version 1.5. The true elemental composition of bulk material for the sample was established by elemental analysis and hence the actual number of counter cations and crystal water molecules was also based on elemental analysis. The resulting formula units were used throughout the manuscript; the CIF file contains the observed chemical formula and the void volume and electron count. The crystallographic data and structure refinement parameters are shown in Table 1. Cambridge crystallographic datafiles CCDC 2 343 046 contain the supplementary crystallographic data for this article. These data can be obtained free of charge from The Cambridge Crystallographic Data Center via www.ccdc.cam.ac.UK/.

Infrared Spectroscopy

The FTIR spectrum was recorded on Shimadzu IRSpirit X-Series FTIR spectrophotometer (Shimadzu Corporation, Japan). The FTIR spectrum of the sample in the solid state was recorded using the KBr pellet technique in the wavenumber range from 4000 to 400 cm^{-1} with 32 scans and 4 cm^{-1} resolution.

Thermogravimetric Analysis

TGA was performed on a TA Instruments Model SDT Q600 thermobalance under nitrogen flow. The temperature was ramped from room temperature to 500 °C at a rate of 5 °C min.

Elemental Analysis

The elemental analyses were conducted using Inductively Coupled Plasma Optical Emission Spectrometry (ICP-OES) method at the Zentrallabor, Technische Universität Hamburg-Harburg (TUHH), Am Schwarzenberg-Campus 1, 21073 Hamburg. The K and Na analyses were performed in-house by atomic absorption (AA) spectroscopy, carried out on a Varian SpectrAA 220 AA spectrometer.

Nuclear Magnetic Resonance Spectroscopy

^{31}P spectra were recorded on a 400 MHz JEOL ECX instrument at room temperature in 5 mm NMR tubes with a resonance frequency of 162 MHz in H_2O/D_2O or toluene. The chemical shift values were reported with respect to the external standard 85% H_3PO_4. Thermal stability studies were performed by in situ heating of the sample in a 5 mm NMR tube and maintaining the temperature throughout the measurement of the spectrum.

X-Ray Photoelectron Spectroscopy

For the XPS sample preparation, a 50 nm-thick gold layer was sputter coated on a silicon substrate. Solution samples were used as such, and solid samples were dispersed in acetone and then drop cast on the gold surface and let to dry. For the photoelectron investigation, the sample was introduced into UHV vessel which had vacuum pressure of 1×10^{-9} mbar and was equipped with a water-cooled X-ray source (Mg/Al-Specs XR 50) and a hemispherical electron analyzer (Specs Phoebos 100). In this experiment, Mg X-Ray radiation was used as source of excitation which had an energy value of 1253.6 eV. A large lens mode was used for the detection of photoelectrons with a pass energy of 30 eV. The obtained data was evaluated by CASATM XPS software and Shirley's method was used to subtract the background.

Raman Spectroscopy

University of Belgrade: The Raman spectra of the samples (solid-state and solution) were recorded on a DXR Raman microscope (Thermo Scientific, USA), using a diode-pumped solid-state laser with an excitation wavelength of 532 nm. The spectra were recorded using

© 2025 The Author(s). ChemistryEurope published by Chemistry Europe and Wiley-VCH GmbH

Research Article
doi.org/10.1002/ceur.202500082

27514765, 2025, 4, Downloaded from https://chemistry-europe.onlinelibrary.wiley.com/doi/10.1002/ceur.202500082 by Technische Universität Hamburg Universitätsbibliothek, Wiley Online Library on [07/11/2025]. See the Terms and Conditions (https://onlinelibrary.wiley.com/terms-and-conditions) on Wiley Online Library for rules of use; OA articles are governed by the applicable Creative Commons License

different laser powers (0.1 to 10 mW) on the sample, 10 s of exposure time and 10 exposures per spectrum, a grating with 900 lines mm^{-1}, and a 50 μm pinhole spectrograph aperture. The solid (powdered) sample was placed on a slide glass while drops of the sample solution (5 μL) were put on a golden plate (Gold EZ spot micro mounts, Thermo Scientific). The laser beam was focused on the sample using an objective magnification ×10.

The thermal treatment of the solid-state sample was performed in a laboratory furnace (ViMS elektrik VMS-10) at 50 and 90 °C under air. The sample was held isothermally for 30 min.

The thermal treatment of the solution (in a closed vessel) was performed by gradual heating in a water bath (the temperature was controlled by a digital thermometer). Aliquots (5 μL) were taken when the target temperature (50 and 90 °C) was reached.

Constructor University: A B&W Tek iRaman Plus spectrometer was used to acquire Raman spectra. A fiber optic probe served for both excitation and signal collection. The spectrometer had an integrated near-infrared laser source (785 nm) for excitation and a charge-coupled detector that can record data in the range from 65 to 3350 cm^{-1}. It was equipped with a fixed low-groove-density grating, which allowed for measurements over a wide spectral range up to 3350 cm^{-1} in a single-detection window.

Additionally, the laser's optical fiber can be placed inside a collimator tube, enabling integration with a microscope apparatus. This arrangement allows for the view and examination of samples with microscopic resolution. A 50× magnification objective was used in this study, resulting in a beam spot size of ≈30–35 mm on the material. A spectral resolution of about 4 cm^{-1} can be achieved with the Raman system. The breathing mode of toluene at 1003.7 cm^{-1} was employed for accurate wavenumber calibration. The BWSpec software was used to control the setup as well as for data acquisition.

Synthesis of $K_{13.6}Na_{1.4}Li[(Ce^{IV}{}_2O_2)Li_2(P_2W_{16}O_{59})_2]\cdot 32H_2O$ (KNaLi-$Ce_2Li_2P_4W_{32}$)

The hexalacunary polyanion precursor salt $K_{12}[\alpha\text{-}H_2P_2W_{12}O_{48}]\cdot 24H_2O$ (**K-P_2W_{12}**) was synthesized according to the published procedure of Contant.[25] All other chemicals were purchased and used without further purification.

K-P_2W_{12} (788 mg, 0.200 mmol) was dissolved in 10 mL 1 M LiCl solution. Then a solution of $Na_2WO_4\cdot 2H_2O$ (264 mg, 0.800 mmol) dissolved in 1 mL water was added and stirred for 2 min at room temperature. The pH of the resultant solution was ≈7.5. A solution of $Ce(NO_3)_3\cdot 6H_2O$ (174 mg, 0.400 mmol) in 400 μL 2 M acetic acid was prepared and slowly added dropwise to the above solution. The pH of the resultant solution was adjusted to 5 with 33% H_2O_2 (≈700 μL) and stirred at 60 °C for 20 min. This solution was filtered at room temperature. After 2 days a white precipitate ($Ce(OH)_3$) was filtered off and the clear solution was then kept for crystallization. Orange crystals were collected after 3 weeks (crystalline yield: 140 mg, 17%), which were then recrystallized by redissolving in a minimum amount of lukewarm water to yield orange crystals of $K_{13.6}Na_{1.4}Li[(Ce^{IV}{}_2O_2)Li_2(P_2W_{16}O_{59})_2]\cdot 32H_2O$ (**KNaLi-$Ce_2Li_2P_4W_{32}$**) upon cooling to room temperature overnight. IR peaks in cm^{-1} (KBr pellet, POM fingerprint region only): 1117 (s), 1077 (s), 1022 (m), 943 (w), 922 (w), 841(w), 793 (w), 737 (w), 627 (w), 495 (b). Elemental analysis (%) calcd: W 62.8, P 1.32, Ce 2.99, K 5.84, Na 0.34, Li 0.22; found: W 63.9, P 1.13, Ce 2.96, K 6.14, Na 0.39, Li 0.21.

Monophasic PPh_3 Reaction

71.4 mg (7.6 μmol) **KNaLi-$Ce_2Li_2P_4W_{32}$** was dissolved in 0.5 mL lukewarm water. Another solution of 4 mg (15.2 μmol) triphenylphosphine in 0.5 mL toluene was prepared and added to the first solution to form a biphasic setup with an orange aqueous phase and colorless toluene phase. An excess of Aliquat 336 was added to this and shaken vigorously for 15 min at room temperature. This transferred the polyanion **$Ce_2Li_2P_4W_{32}$** to toluene as indicated by the transfer of the orange color from the aqueous phase to toluene and the former eventually became colorless. Then the water was removed by decantation and the toluene phase with PPh_3 and **$Ce_2Li_2P_4W_{32}$** was heated to 70 °C and the reaction was monitored over time by ^{31}P NMR.

Acknowledgements

U.K. is thankful to the German Science Foundation (DFG, KO-2288/31-1, KO-2288/29-1, and KO-2288/26-1) and Constructor University for research support. G.Ć.-M. and D.B.-B. thank the Ministry of Science, Technological Development and Innovation of the Republic of Serbia (contract 451-03-137/2025-03/200146), for support. The POM structural images were generated by Diamond, version 3.2 (software copyright, Crystal Impact GbR).

Conflict of Interest

The authors declare no conflict of interest.

Data Availability Statement

The data that support the findings of this study are available in the supplementary material of this article.

Keywords: cerium · oxidation · Raman spectroscopy · peroxo-species · polyoxometalates

[1] a) M. T. Pope, *Heteropoly and Isopoly Oxometalates*, Springer-Verlag, Berlin **1983**; b) P. Yang, U. Kortz, *Comprehensive Coordination Chemistry III*; (Eds: E. C. Constable, G. Parkin, L. Que Jr.), Elsevier, Amsterdam, Oxford, Cambridge, MA **2021**, *7*, 4.
[2] C. Venturello, R. D'Aloisio, J. C. J. Bart, M. A. Ricci, *J. Mol. Catal.* **1985**, *32*, 107.
[3] C. A. Ohlin, E. M. Villa, J. C. Fettinger, W. H. Casey, *Angew. Chem. Int. Ed.* **2008**, *47*, 8251.
[4] a) J.-Y. Piquemal, L. Salles, G. Chottard, P. Herson, C. Ahcine, J.-M. Brégeault, *Eur. J. Inorg. Chem.* **2006**, *2006*, 939; b) J. Server-Carrió, J. Bas-Serra, M. E. González-Núñez, A. García-Gastaldi, G. B. Jameson, L. C. W. Baker, R. Acerete, *J. Am. Chem. Soc.* **1999**, *121*, 977.
[5] a) A. Sundar, N. V. Maksimchuk, I. D. Ivanchikova, O. V. Zalomaeva, D. Bajuk-Bogdanović, O. A. Kholdeeva, G. Ćirić-Marjanović, B. S. Bassil, U. Kortz, *Chem. Eur.* **2024**, *2*, e202300066; b) S. S. Mal, N. H. Nsouli, M. Carraro, A. Sartorel, G. Scorrano, H. Oelrich, L. Walder, M. Bonchio, U. Kortz, *Inorg. Chem.* **2010**, *49*, 7; c) B. S. Bassil, S. S. Mal, M. H. Dickman, U. Kortz, H. Oelrich, L. Walder, *J. Am. Chem. Soc.* **2008**, *130*, 6696; d) O. A. Kholdeeva, G. M. Maksimov, R. I. Maksimovskaya, M. P. Vanina, T. A. Trubitsina, D. Y. Naumov, B. A. Kolesov, N. S. Antonova, J. J. Carbó, J. M. Poblet, *Inorg. Chem.* **2006**, *45*, 7224.
[6] a) M. T. Pope, *Handbook on the Physics and Chemistry of Rare Earth*, (Eds: K. A. Gschneidner, L. Eyring) North-Holland Publ. Co., Amsterdam, **2008**, 337; b) M. Zimmermann, N. Belai, R. J. Butcher, M. T. Pope, E. V. Chubarova, M. H. Dickman, U. Kortz, *Inorg. Chem.* **2007**, *46*, 1737; c) N. Belai, M. H. Dickman, M. T. Pope, R. Contant, B. Keita, I-M. Mbomekalle, L. Nadjo, *Inorg Chem.* **2005**, *44*, 169; d) A. Ostuni, M. T. Pope, *C. R. Acad. Sci. Paris, Série IIc, Chimie*, **2000**, *3*, 199; e) K. Wassermann, M. H. Dickman, M. T. Pope, *Angew. Chem. Int. Ed.* **1997**, *36*, 1445;

© 2025 The Author(s). ChemistryEurope published by Chemistry Europe and Wiley-VCH GmbH

Research Article
doi.org/10.1002/ceur.202500082

f) I. Creaser, M. C. Heckel, R. J. Neitz, M. T. Pope, *Inorg. Chem.* **1993**, *32*, 1573.
[7] a) C. Zhang, L. Bensaid, D. McGregor, X. Fang, R. C. Howell, B. Burton-Pye, Q. Luo, L. Todaro, L. C. Francesconi, *J. Cluster Sci.* **2006**, *17*, 389; b) C. Boglio, G. Lenoble, C. Duhayon, B. Hasenknopf, R. Thouvenot, C. Zhang, R. C. Howell, B. P. Burton-Pye, L. C. Francesconi, E. Lacôte, S. Thorimbert, M. Malacria, C. Afonso, J.-C. Tabet, *Inorg. Chem.* **2006**, *45*, 1389; c) C. Zhang, R. C. Howell, K. B. Scotland, F. G. Perez, L. Todaro, L. C. Francesconi, *Inorg. Chem.* **2004**, *43*, 7691; d) M. R. Antonio, L. Soderholm, C. W. Williams, N. Ullah, L. C. Francesconi, *J. Chem. Soc., Dalton Trans.* **1999**, *21*, 3825; e) J. Bartis, M. Dankova, J. J. Lessmann, Q.-H Luo, W. D. Horrocks, L. C. Francesconi, *Inorg. Chem.* **1999**, *38*, 1042.
[8] a) J. Qiu, P. C. Burns, *Chem. Rev.* **2012**, *113*, 1097; b) J. Ling, J. Qiu, P. C. Burns, *Inorg. Chem.* **2012**, *51*, 2403; c) M. Nyman, P. C. Burns, *Chem. Soc. Rev.* **2012**, *41*, 7354; d) G. E. Sigmon, J. Ling, D. K. Unruh, L. Moore-Shay, M. Ward, B. Weaver, P. C. Burns, *J. Am. Chem. Soc.* **2009**, *131*, 16648; e) T. Z. Forbes, J. G. McAlpin, R. Murphy, P. C. Burns, *Angew. Chem. Int. Ed.* **2008**, *47*, 2824; f) K. A. Kubatko, P. C. Burns, *Inorg. Chem.* **2006**, *45*, 6096.
[9] H. M. Qasim, W. W. Ayass, P. Donfack, A. S. Mougharbel, S. Bhattacharya, T. Nisar, T. Balster, A. Solé-Daura, I. Römer, J. Goura, A. Materny, V. Wagner, J. M. Poblet, B. S. Bassil, U. Kortz, *Inorg. Chem.* **2019**, *58*, 11300.
[10] a) H. Aoto, K. Matsui, Y. Sakai, T. Kuchizi, H. Sekiya, H. Osada, T. Yoshida, S. Matsunaga, K. Nomiya, *J. Mol. Catal. A Chem.* **2014**, *394*, 224; b) R. Neumann, M. Gara, *J. Am. Chem. Soc.* **1995**, *117*, 5066.
[11] a) N. V. Maksimchuk, V. Y. Evtushok, O. V. Zalomaeva, G. M. Maksimov, I. D. Ivanchikova, Y. A. Chesalov, I. V. Eltsov, P. A. Abramov, T. S. Glazneva, V. V. Yanshole, O. A. Kholdeeva, R. J. Errington, A. Solé-Daura, J. M. Poblet, J. J. Carbó, *ACS Catal.* **2021**, *11*, 10589; b) N. V. Maksimchuk, I. D. Ivanchikova, G. M. Maksimov, I. V. Eltsov, V. Y. Evtushok, O. A. Kholdeeva, D. Lebbie, R. J. Errington, A. Solé-Daura, J. M. Poblet, J. J. Carbó, *ACS Catal.* **2019**, *9*, 6262; c) N. V. Maksimchuk, G. M. Maksimov, V. Y. Evtushok, I. D. Ivanchikova, Y. A. Chesalov, R. I. Maksimovskaya, O. A. Kholdeeva, A. Solé-Daura, J. M. Poblet, J. J. Carbó, *ACS Catal.* **2018**, *8*, 9722; d) P. Jiménez-Lozano, I. D. Ivanchikova, O. A. Kholdeeva, J. M. Poblet, J. J. Carbó, *Chem. Commun.* **2012**, *48*, 9266; e) M. Carraro, A. Sartorel, M. Ibrahim, N. Nsouli, C. Jahier, S. Nlate, U. Kortz, M. Bonchio, *Innovative Catalysis in Organic Synthesis: Oxidation, Hydrogenation, and C—X Bond Forming Reactions*, (Ed. P. G. Andersson), Wiley-VCH: Weinheim, Germany **2012**; f) B. G. Donoeva, T. A. Trubitsina, N. S. Antonova, J. J. Carbó, J. M. Poblet, G. Al-Kadamany, U. Kortz, O. A. Kholdeeva, *Eur. J. Inorg. Chem.* **2010**, 5312; g) N. S. Antonova, J. J. Carbó, U. Kortz, O. A. Kholdeeva, J. M. Poblet, *J. Am. Chem. Soc.* **2010**, *132*, 7488; h) O. A. Kholdeeva, B. G. Donoeva, T. A. Trubitsina, G. Al-Kadamany, U. Kortz, *Eur. J. Inorg. Chem.* **2009**, 5134; i) F. Hussain, B. S. Bassil, U. Kortz, O. A. Kholdeeva, M. N. Timofeeva, P. de Oliveira, B. Keita, L. Nadjo, *Chem. Eur. J.*, **2007**, *13*, 4733.
[12] W. N. Lipscomb, *Inorg. Chem.* **1965**, *4*, 132.
[13] R. Massart, R. Contant, J.-M. Fruchart, J.-P. Ciabrini, M. Fournier, *Inorg. Chem.* **1977**, *16*, 2916.
[14] I. D. Brown, D. Altermatt, *Acta Crystallogr., Sect. B: Struct. Sci.* **1985**, *41*, 244.
[15] S. S. Mal, M. H. Dickman, U. Kortz, *Chem. Eur. J.* **2008**, *14*, 9851.
[16] a) C. Rocchiccioli-Deltcheff, R. Thouvenot, *Spectrosc. Lett.* **1979**, *12*, 127; b) R. Thouvenot, M. Fournier, R. Franck, C. Rocchiccioli-Deltcheff, *Inorg. Chem.* **1984**, *23*, 598.
[17] D. D. Agarwal, R. Jain, R. P. Bhatnagar, S. Srivastava, *Polyhedron* **1990**, *9*, 1405.
[18] a) R. Haegele, J. C. A. Boeyens, *J. Chem. Soc. Dalt. Trans.* **1977**, *7*, 648; b) A. Misra, K. Kozma, C. Streb, M. Nyman, *Angew. Chem. Int. Ed.* **2020**, *59*, 596.
[19] a) S. Venkateswaran, *Nature* **1931**, *127*, 406; b) G. V. Jere, M. T. Santhamma, *Inorg. Chim. Acta* **1977**, *24*, 57.
[20] G. Socrates, *Infrared and Raman Characteristic Group Frequencies: Tables and Charts*. John Wiley & Sons: Chichester **2004**, 321.
[21] Rigaku. *CrysAlisPro Software System*, version 1.171.38.41; Rigaku Oxford Diffraction.
[22] Rigaku. ABSPACK, SCALE. "Empirical Absorption correction." CrysAlis Pro–Software Package; Rigaku Oxford Diffraction **2022**.
[23] G. M. Sheldrick, *SHELX, Program for Solution of Crystal Structures*, University of Göttingen, Germany **2015**.
[24] O. V. Dolomanov, L. J. Bourhis, R. J. Gildea, J. A. K. Howard, H. Puschmann, *J. Appl. Cryst.* **2009**, *42*, 339.
[25] R. Contant, *Inorganic Syntheses*, (Ed. A. P. Ginsberg) John Wiley and Sons, New York **1990**, 104.

Manuscript received: March 29, 2025
Revised manuscript received: April 29, 2025
Version of record online: June 3, 2025

© 2025 The Author(s). ChemistryEurope published by Chemistry Europe and Wiley-VCH GmbH

27514765, 2025, 4, Downloaded from https://chemistry-europe.onlinelibrary.wiley.com/doi/10.1002/ceur.202500082 by Technische Universität Hamburg Universitätsbibliothek, Wiley Online Library on [07/11/2025]. See the Terms and Conditions (https://onlinelibrary.wiley.com/terms-and-conditions) on Wiley Online Library for rules of use; OA articles are governed by the applicable Creative Commons License